JOURNAL OF AIRCRAFT
Vol. 35, No. 3, May–June 1998

Drag Reduction and Shape Optimization of Airship Bodies

T. Lutz* and S. Wagner†
University of Stuttgart, Stuttgart D-70550, Germany

A tool for the numerical shape optimization of axisymmetric bodies submerged in incompressible flow at zero incidence has been developed. Contrary to the usual approach, the geometry of the body is not optimized in a direct way with this method. Instead, a source distribution on the body axis was chosen to model the body contour and the corresponding inviscid flowfield, with the source strengths being used as design variables for the optimization process. Boundary-layer calculation is performed by means of a proved integral method. To determine the transition location, a semiempirical method based on linear stability theory (e^n method) was implemented. A commercially available hybrid optimizer as well as an evolution strategy with covariance matrix adaption of the mutation distribution are applied as optimization algorithms. Shape optimizations of airship hulls were performed for different Reynolds number regimes. The objective was to minimize the drag for a given volume of the envelope and a prescribed airspeed range.

Nomenclature

A = amplitude of a Tollmien–Schlichting wave
c_{d_V} = volumetric drag coefficient
c_P = pressure coefficient
D = drag
f = frequency
H_{32} = shape factor
N = total number of source sections
n = amplification factor
q_{0_i} = source strength at the beginning of the ith section
q_{1_i} = source strength at the end of the ith section
Re = Reynolds number
Re_L = Reynolds number based on body length
Re_V = volumetric Reynolds number
r_{0_i} = distance from start of ith source section to field point
r_{1_i} = distance from end of ith source section to field point
s = arc length
t = time
U = basic flow
U_∞ = undisturbed freestream velocity
V = body volume
w_r = radial velocity component
w_x = axial velocity component
x, r = coordinates of the cylindrical coordinate system
α_i = amplification rate
α_r = wave number
Δx_i = length of ith source section
ν = kinematic viscosity
ρ = density of the fluid
Φ = velocity potential
ς = eigenfunction
Ψ = stream function
ω = circular frequency

Indices
A = field point
crit = critical value
I = value at the primary instability point
V = quantity based on body volume

Received May 10, 1997; presented as Paper 97-1483 at the AIAA 12th Lighter-Than-Air Systems Technology Conference, San Francisco, CA, June 3–5, 1997; revision received Oct. 30, 1997; accepted for publication Nov. 8, 1997.

*Research Assistant, Institute for Aerodynamics and Gasdynamics, Pfaffenwaldring 21.

†Professor, Head of Institute, Institute for Aerodynamics and Gasdynamics, Pfaffenwaldring 21. Member AIAA.

I. Introduction

IN the process of developing new airships, the current central topics are reliable construction and safe operation. If future airships for long endurance missions or transportation purposes are realized, economical operation will be important. It will then be most important to minimize the weight and power requirements of the configuration. The required propulsive power depends mainly on the aerodynamic drag of the airship hull, which accounts for about two-thirds of the total drag. Even a small reduction in hull drag can result in a significant fuel savings, which in turn, will lead to a greater payload capacity or an increased range of the airship. During the aerodynamic design of an airship it is therefore important to find a drag-minimized envelope for the intended range of missions.

First, systematic investigations on the drag of axisymmetric bodies were conducted by Gertler.[1] The objective of his experimental work was the determination of a low-drag submarine contour. Because no extensive laminar flow regions were expected for this application, no special laminar shapes were examined in this research study.

The question concerning drag reduction by extended laminar flow regions at medium Reynolds numbers was investigated by Carmichael,[2] by means of drop-tests carried out in the Pacific Ocean. He was able to prove that for $Re_L = 10–40 \times 10^6$ extensive laminar flow is possible. For the body examined, a reduction of the volumetric drag coefficient of up to 60% could be achieved compared to conventional turbulent body shapes.

Further experimental research on laminar bodies for low Reynolds number applications was conducted by Hansen and Hoyt.[3] During the experiments a high sensitivity of the transition location to even the smallest surface roughnesses was observed, which restricts practical applications of such extensive laminar bodies.

There are very few experimental investigations on the drag of axisymmetric bodies at large Reynolds numbers ($Re_V > 10^7$). Therefore, mainly theoretical methods are relied on. Numerical shape optimizations were performed by Parsons et al.[4] The utilized calculation model is based on a panel code that was coupled with a boundary-layer method.

In contrast, Zedan et al.[5] applied an inverse method based on a linearly varying doublet distribution on the body axis for the design of low-drag aircraft fuselages. The fuselage de-

signed shows a long region with a favorable pressure gradient in its forward section. It was stated that this should result in laminar flow up to 70% of the body length at Reynolds numbers of $Re_V = 10\text{–}30 \times 10^6$. Further numerical shape optimizations were carried out by Dodbele et al.,[6] Coiro and Nicolosi,[7] and Pinebrook.[8]

Most publications on shape optimization are concerned with the design of bodies with extended laminar flow. An exception in this respect is the research done by Hess and James,[9] who conducted drag computations for bodies of revolution where the boundary layer was fully turbulent. Their disillusioning conclusion was that the volumetric drag coefficient is very insensitive to changes in body contour and, thus, that no significant drag reduction can be obtained from shaping alone in case of a fully turbulent boundary layer.

Shape optimizations of axisymmetric bodies for different Reynolds numbers were presented by the authors.[10] To perform these investigations, an indirect potential method had been coupled with an integral boundary-layer method and an evolution strategy as optimization algorithm.[11] An empirical local transition criterion was used because of the small amount of required computing time. Analysis of the optimized geometries using a more sophisticated e^n method resulted partly in considerably different transition locations and confirmed the inadequacies of local criteria. For this reason, a costly e^n method has also been recently implemented in the optimization tool.

The present paper describes the improved aerodynamic design and analysis method and gives examples of the validation. After that, the optimization algorithms that had been coupled with the aerodynamic code are presented. Compared to previous investigations,[10,11] a new step-size adaption was incorporated into the evolution strategy and a commercially available hybrid optimizer was implemented. The complete tool has been used for the shape optimization of axisymmetric bodies for a variety of Reynolds number regimes. The selection of the design variables, the definition of the objective function and the resulting body shapes are discussed within this paper.

II. Flow Calculation

For the present investigations potential-flow methods were coupled with an integral boundary-layer code to calculate the drag of bodies of revolution at zero incidence. During the shape optimization process, the inviscid flowfield is computed by means of an efficient inverse method based on a linearly varying source distribution on the body axis. In contrast, a three-dimensional panel method was used to analyze the flow about given body shapes. There was special emphasis on the determination of the transition point, because the length of the laminar flow region has a substantial impact on the drag coefficient, particularly for small to medium Reynolds numbers. A transition prediction method that is as reliable and consistent as possible is of essential importance for the successful shape optimization of laminar bodies. Hence, the transition criterion employed will be discussed in more detail.

A. Inviscid Formulation

1. Design Procedure

Based on the assumption of an isentropic and irrotational flowfield, a velocity potential Φ can be introduced. The continuity equation supplies the equation for the determination of Φ, which assumes the form of the Laplace equation in case of an incompressible fluid:

$$\Delta\Phi = 0 \tag{1}$$

As this potential equation represents a partial *linear* differential equation, a superposition of elementary solutions such as source or doublet singularities is possible. The flow about a body of revolution at zero incidence can be modeled by superimposing the flowfield of a source distribution on the body axis with that of a parallel onset flow. The present approach uses a source distribution varying linearly by section, as proposed by Zedan and Dalton[12] (Fig. 1).

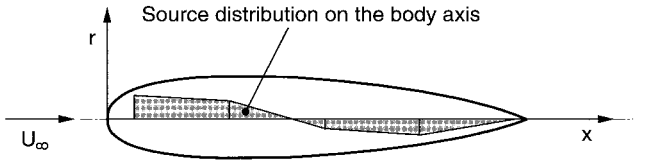

Fig. 1 Modeling of the flowfield by means of a source distribution on the body axis.

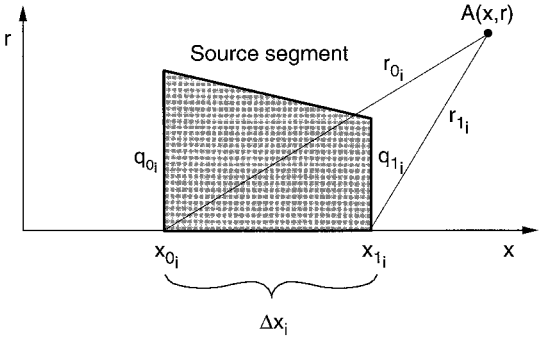

Fig. 2 Source section with linearly varying strength.

Because of the rotational symmetry of the flowfield, a stream function Ψ with the two independent variables x and r can be introduced. For a number of N source sections the value Ψ_A of the stream function in the field point $A(x, r)$ for a number of N source sections results in

$$\begin{aligned}\Psi_A = \frac{U_\infty}{2} r^2 - \frac{1}{8\pi} \sum_{i=1}^{N} \frac{1}{\Delta x_i} \{ &(q_{1_i} - q_{0_i}) r^2 \ell n\, \kappa \\ &+ [q_{1_i}(x - x_{0_i}) - q_{0_i}(x + x_{0_i} - 2x_{1_i})] r_{0_i} \\ &+ [q_{0_i}(x - x_{1_i}) - q_{1_i}(x + x_{1_i} - 2x_{0_i})] r_{1_i} \}\end{aligned} \tag{2}$$

where

$$\kappa = \frac{x - x_{0_i} + r_{0_i}}{x - x_{1_i} + r_{1_i}}$$

Here, q_{0_i} represents the source strength at the beginning, q_{1_i} the source strength at the end, and Δx_i the length of the ith segment (Fig. 2). The distance between field point A and the segment boundaries is designated by r_{0_i} or r_{1_i}, respectively.

Because the body surface is identical to the stagnation stream surface, the defining equation for the contour is obtained by setting Eq. (2) equal to the value of the stream function in the stagnation points. Using this defining equation, the body geometry can be determined by means of an iterative procedure. To generate closed contours, the closure condition has to be satisfied. This condition implies that the integral of the source strength has to be zero at the body tail.

The inviscid velocity field results from differentiation of the stream function. Thus, the axial radial velocity component at an arbitrary field point $A(x, r)$ respectively follows from Eq. (2):

$$w_{x_A} = U_\infty - \frac{1}{4\pi} \sum_{i=1}^{N} \left(\frac{q_{0_i}}{r_{0_i}} - \frac{q_{1_i}}{r_{1_i}} + \frac{q_{1_i} - q_{0_i}}{\Delta x_i} \ell n\, \kappa \right) \tag{3}$$

$$\begin{aligned}w_{r_A} = -\frac{1}{4\pi} \sum_{i=1}^{N} \frac{r}{\Delta x_i} \Bigg\{ &(q_{1_i} - q_{0_i}) \left(\frac{1}{r_{1_i}} - \frac{1}{r_{0_i}} \right) \\ &+ [q_{1_i}(x - x_{0_i}) - q_{0_i}(x - x_{1_i})] \\ &\times \left[\frac{1}{r_{0_i}(x - x_{0_i} + r_{0_i})} - \frac{1}{r_{1_i}(x - x_{1_i} + r_{1_i})} \right] \Bigg\}\end{aligned} \tag{4}$$

For a prescribed source distribution this potential method enables an exact and very efficient calculation of the body contour and the corresponding inviscid flowfield. However, it should be emphasized that not all imaginable body shapes can be modeled. For example, bodies with sharp corners or geometries with a length-to-diameter (L/D) ratio smaller than 1 must be excluded. Such blunt, separation-prone bodies will not be discussed in the scope of this paper because of their inferior aerodynamic characteristics.

2. Analysis Procedure

To solve the direct problem, i.e., to calculate the inviscid velocity distribution for given body shapes, a panel method is applied. In this analysis method source singularities with panelwise constant strength are used, with the singularity distribution being determined by application of the external Neumann boundary condition. This low-order approach is sufficient when using an adequately fine discretization of the body geometry. A modified Bèzier spline serves for the interpolation of geometry and velocity distribution and provides the input data for the boundary-layer calculation.

B. Boundary-Layer Method

The boundary-layer calculation is performed based on the inviscid velocity distribution on the body surface that results from the design or analysis procedure described earlier. For the present investigations, an integral method according to Eppler and Somers[13] was applied. This code was expanded for the calculation of axisymmetric boundary layers. Curvature effects are neglected with the first-order method. This simplification seems permissible because the boundary-layer thickness in the Reynolds number range investigated is much smaller than the curvature radii. An exception to this is the area around the body tail.

For transition prediction a semiempirical e^n method has been implemented, which will be described in more detail in the following section. If laminar separation occurs upstream of transition, the boundary-layer method switches to turbulent closure relations at the separation point. The additional drag resulting from laminar separation bubbles is not determined. With the design procedure, the displacement effect of the boundary layer is neglected, whereas the panel method enables an iterative viscous/inviscid coupling by application of the transpiration technique.

The drag coefficient is determined by using the formula of Young,[14] which takes the skin friction and form drag of attached boundary layers into account.

C. Transition Prediction

At low freestream turbulence level, the boundary layer starting at the stagnation point is initially laminar and stable against perturbations. Downstream of the primary instability point, disturbance waves with small amplitude (Tollmien–Schlichting waves) are being amplified, i.e., their amplitude grows in downstream direction. After this region of linear instability, nonlinear interaction of different disturbance waves occurs. This secondary instability initiates the subsequent stages of the transition process, which leads to a rapid breakdown to turbulence.

The amplification of sinusoidal disturbance waves of small amplitude can be calculated by means of the linear stability theory in very good agreement with experimental results. This theory can be used to derive predictions about the onset of transition, because the region of nonlinear amplification is short if compared to the region of linear instability.

1. Linear Stability Theory for Two-Dimensional, Incompressible Flow

The first basic assumption of the linear stability theory is to separate the two-dimensional boundary-layer flow into a steady basic flow $U(y)$ and an unsteady disturbance. Furthermore, local parallelism is assumed. The basic flow represents a steady solution of the Navier–Stokes equation, whereas for the disturbance a harmonic wave approach is chosen, which can be described by means of the following stream function:

$$\Psi = \varsigma(y)e^{i(\alpha x-\omega t)} + \text{complex conjugate} \tag{5}$$

In this equation, y represents the distance normal to the wall. The perturbation velocity components in streamwise and normal direction result from differentiation of the stream function. Substitution of the disturbance velocities into the complete Navier–Stokes equation, elimination of the pressure variable and linearization result in the Orr-Sommerfeld equation, which can be expressed in the following form[15]:

$$(D^2 - \alpha^2)^2\varsigma = i\alpha Re\left[\left(U - \frac{\omega}{\alpha}\right)(D^2 - \alpha^2) - D^2U\right]\varsigma \tag{6}$$

where

$$D = \frac{\mathrm{d}}{\mathrm{d}y} \tag{7}$$

Here, we consider spatial growth of the Tollmien–Schlichting waves. In this case, ω represents a real quantity and stands for the circular frequency of the disturbance waves. In contrast, α is complex with its real part α_r being the wave number and its imaginary part α_i being the amplification rate. Negative values for α_i indicate a spatial amplification, whereas positive values mean decay of the perturbation wave amplitude. Because the boundary conditions of Eq. (6) are homogeneous, an eigenvalue problem results. Now the amplitude development of a Tollmien–Schlichting wave with circular frequency ω can be evaluated for a given boundary-layer profile of the steady basic flow and a specified local Reynolds number.

The linear stability theory, as described has been derived for a plane flow. Because in the present investigations the boundary-layer thickness is much smaller than the radius over the entire body, this approach can be applied for axisymmetric boundary layers as well.

2. Semiempirical e^n Method

Various authors refer to the deficiencies of simple local transition criteria for the evaluation of the transition point of airfoil sections and axisymmetric bodies.[5,6,16] For slender bodies with a flat pressure distribution, a wide range of transition locations can be found with different criteria. Less scattering in comparison to wind-tunnel measurements results with nonlocal criteria such as the e^n method, which is based on linear stability theory. This method was developed independently by Smith and Gamberoni[17] and van Ingen.[18] With the e^n method, transition is assumed, when the amplification factor n for a certain frequency of the Tollmien–Schlichting waves reached a critical value n_{crit}:

$$n = \ell n\frac{A}{A_I} = -\int_{s_I}^{s}\alpha_i(f)\,\mathrm{d}s \geq n_{\text{crit}} \tag{8}$$

In Eq. (8) A/A_I describes the ratio of the local amplitude A of the perturbation wave to the amplitude A_I in the primary instability point s_I. The critical amplification factor is assumed to be dependent on the freestream conditions. Based on comparisons of experimentally found and theoretically obtained transition locations, Mack[19] and van Ingen and Boermans[20] presented correlations for n_{crit}, depending on the freestream turbulence level. Note that the process of receptivity and the magnitude of the initial disturbance amplitude is not considered. Furthermore, the method fails if large-amplitude perturbations enter the boundary layer and the linear stages of the transition process are bypassed.

In the present implementation, the boundary-layer profiles required for the computation of the amplification rates are ob-

tained from a polynomial approximation of the Falkner-Skan profiles. This approach is practical, because the laminar boundary-layer method used is based on the similar solutions of the boundary-layer equations. The shape factor H_{32} serves as a coupling parameter. At each coordinate downstream of the primary instability point, the spatial amplification rates α_i are calculated for a multitude of physical frequencies. After that, the amplification rate is integrated along the arc length of the body for each of these frequencies. Subsequently, the envelope is evaluated for the resulting amplification curves. Transition is finally assumed at the position where the envelope exceeds the specified critical value of n_{crit} (Fig. 3).

Calculating the amplification rate by solving the complete Orr–Sommerfeld equation is costly as well as problematic in highly damped regions. Therefore, the frequency spectrum is adjusted dynamically in the present analysis method. This means that stability analysis for a specific f is only performed if the amplification rate $\alpha_i(f)$ is negative or the total amplification factor $n(f)$ is greater than zero. This procedure still requires too much computational effort for the purpose of numerical shape optimization. For this reason, a simplified method has been implemented, which can be used alternatively. With this method, the amplification rate for many shape factors, Reynolds numbers, and frequencies is calculated by solving the Orr–Sommerfeld equations in advance. The results are stored in a database, from which the required amplification rates can be interpolated during the actual transition calculations. For the present implementation a database containing α_i values for 27 shape factors at 40 different Reynolds numbers and 40 different frequencies has been generated.

D. Validation of the Calculation Method

The analysis method described in the previous sections has been verified with regard to drag computation for various bodies of revolution. As an example, Fig. 4 shows the calculated drag curve for Gertler body 4154, which represents a shape similar to an airship hull. The theoretical drag curve is compared to results of water-tunnel tests performed by Gertler.[1] The transition point has been fixed at 5% of the body length in both the experimental investigation and the calculation. Good agreement for the whole Reynolds number range examined has been achieved.

The validation for axisymmetric bodies with natural transition is difficult because only very few experiments at large Reynolds numbers are known. In Fig. 5 experimental results of Jones respectively Schirmer[21] for the R101 airship body are depicted. These very old measurements must be examined with caution because the formerly available wind tunnels featured a relatively high level of freestream turbulence. In case of the LZ windtunnel of the former Zeppelin company, in which

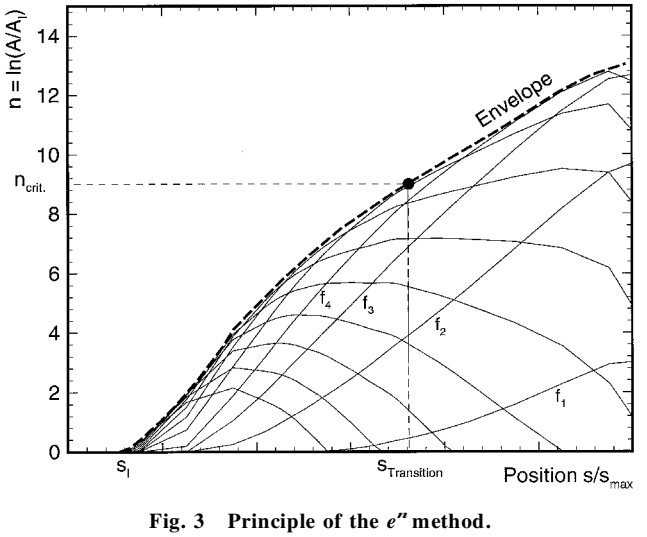

Fig. 3 Principle of the e^n method.

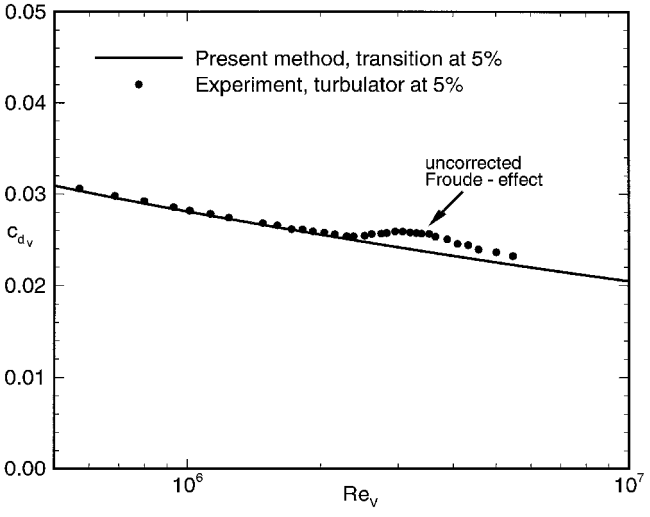

Fig. 4 Drag curve for Gertler body 4154 (Ref. 1).

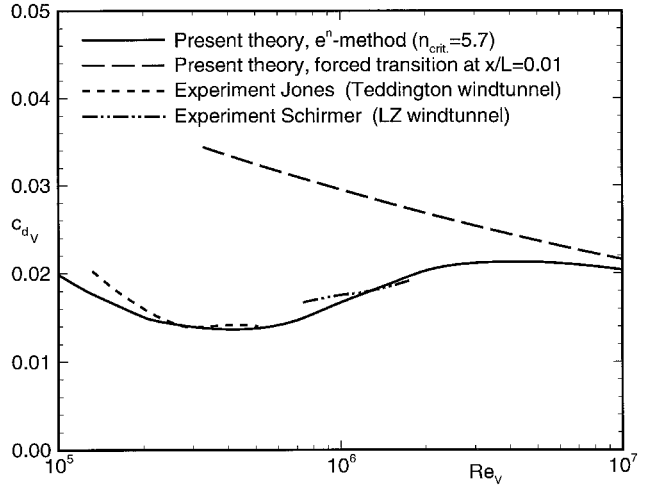

Fig. 5 Drag curve for the R101 airship body.[21]

Schirmer conducted his experiments, there was a turbulence factor of 1.35. This corresponds to a turbulence level of approximately 0.45%, for which a factor of $n_{crit} = 5.7$ results from the correlation according to van Ingen and Boermans.[20] The theoretically obtained drag curve for that value of n_{crit} shows satisfactory agreement with the experimental results (Fig. 5).

III. Numerical Shape Optimization Procedure

A. Optimization Algorithms

The aerodynamical optimization problem presented is first characterized by the fact that the gradient of the objective function (drag coefficient) cannot be determined analytically. Furthermore, the objective function is expected to be multimodal, i.e., it shows more than one minimum within the design space. The optimization algorithm must therefore be efficiently applicable to such multidimensional, multimodal, and nonlinear objective functions. In addition, the algorithm should be robust, i.e., processing of optimization problems with complex topology of the objective function should be possible. Experience shows that the subject last mentioned is particularly important for shape optimizations of laminar bodies. In the vicinity of the optimum, even smallest variations of the design variables can trigger an upstream jump of the theoretical transition location. This increases the drag coefficient drastically, which is equivalent to a jump of the objective function value.

Various optimization strategies were applied to obtain the results presented in Sec. IV. First, the commercially available tool POINTER was used, which enables constrained optimi-

zation. This hybrid optimizer is composed of a combination of genetic algorithm (GA), downhill simplex, and gradient methods. A search procedure suitable for the optimization task at hand was chosen by means of automated training sessions with the desired optimization time being specified. The algorithm applied by the program, the number of iterations and restarts, as well as the step-sizes are not known to the user.

The second optimization tool is an evolution strategy[22] with derandomized covariance matrix adaption implemented for a generalized individual mutation step-size control.[23] The classical evolution strategy as well as genetic algorithms are optimization methods that take reference to the biological evolution process. Mechanisms such as recombination, random mutation and selection are adopted to generate new design vectors from a given pool of inital designs.[22] For the shape optimizations presented, a simple (1, 30)-selection strategy was used. With this strategy one parent design produces 30 offspring individuals from which the best one is selected as a parent of the next generation.

Of crucial importance for the success of an optimization is the self-adaption of the step-size that is used for mutation of the design variables. In the method applied, the mutation step-size and the mutation distribution is adjusted according to the selection information acquired along an entire evolution path. This means that during the evolution process the optimization tool learns which order of magnitude the mutation step-size and the direction for the individual design variables should be. The method is characterized by a high convergence rate, even for complex objective functions, after successful adaption of the covariance matrix.

B. Representation of the Body Shape

Contrary to the usual approach, the geometry of the body is not optimized in a direct way in the investigations presented here. Rather, the design method described in Sec. II.A is applied with the source distribution on the body axis being varied by the optimizer. The indirect method has been chosen because it requires significantly less computation time compared to panel methods in case of a great number of collocation points. The procedure is essentially similar to the method of Pinebrook,[8] who performed shape optimizations of axisymmetric bodies to minimize the drag coefficient based on frontal area.

In the investigations presented in Sec. IV, the lengths Δx_i of $N = 20$ source segments are optimized along with the source strength q_{0_i} at the beginning of each segment and the strength q_{1_N} at the end of the last segment. To prevent negative values for Δx_i, a logarithmic scale is introduced, so that the following set of design variables results:

$$q_{0_i} \quad \text{with} \quad i = [1, 2, \ldots, N]$$

$$\log(\Delta x_i) \quad \text{with} \quad i = [1, 2, \ldots, N]$$

$$q_{1_N}$$

To ensure a continuous singularity distribution, the source strengths q_{1_i} at the end of the segment boundaries are set equal to the value $q_{0_{i+1}}$ at the beginning of the following segment.

With the indirect method chosen, the closure condition has to be fulfilled exactly to enable the calculation of the rear stagnation point. Introducing a constraint might not yield an exact realization of this condition because the used optimizer deals with constraints by imposing a penalty upon the objective function. Therefore, the source distribution generated by the optimizer is superimposed by a parabolic correction distribution. Even if the closure condition is satisfied, it is possible that in some cases negative values for the source-strength integral within the singularity distribution result. This would lead to inadmissible solutions. To avoid such designs as far as possible, proper constraints are used.

It should be noted that no geometric constraints are introduced within the present shape optimizations. This means that the optimization process is driven solely by the aerodynamic objective to minimize drag.

C. Optimization Target and Objective Function

The optimization target relevant for the aerodynamic design of airship hulls is to achieve minimum drag at specified hull volume and airspeed.[24] During the investigation of this question the following dimensionless quantities are relevant when comparing different configurations:
Volumetric drag coefficient:

$$c_{d_V} = \frac{D}{(\rho/2)U_\infty^2 V^{2/3}} \tag{9}$$

Volumetric Reynolds number:

$$Re_V = \frac{U_\infty V^{1/3}}{\nu} \tag{10}$$

An inconsistent choice of the reference length leads to wrong results if drag coefficients for different configurations are compared.[24]

Previous investigations[10] showed that one-point optimizations for a single Reynolds number lead to bodies that are inconvenient or even unusable outside of their design point. This is especially true for laminar bodies at low Reynolds numbers. Therefore, the weighted mean value c_{d_V} of the drag coefficients for a whole Re_V regime was chosen as the objective function to be minimized. The total drag coefficient defining the fitness is developed with the friction and form drag of the attached boundary layer. Additionally, a penalty function is introduced representing an estimation of the pressure drag in case of turbulent separation. The estimation is based on the pressure force resulting from integration of the inviscid pressure distribution with a constant value of c_p being assumed downstream of the separation point. Because the implemented penalty function is pessimistic, bodies with negligible separated flow regions result during the optimization process. Using a continuous estimation of the pressure drag instead of discarding designs with separation upstream of a certain location results in accelerating the optimization process and leads to reasonable tail geometries.

IV. Results and Discussion

When plotting the drag coefficient of an axisymmetric body vs Reynolds number, three different regions can be distinguished. At low Reynolds numbers, extensive laminar flow is possible, which results in low skin friction. With increasing Reynolds number the transition point moves more or less rapidly toward the body nose, thereby increasing the drag coefficient (Fig. 5). The large Reynolds number regime can be characterized by the fact that the boundary layer is almost fully turbulent.

An important task of aerodynamics is to determine how to shape the body geometry to delay transition and minimize the drag coefficient. This question has been examined for different Reynolds number regimes by application of the optimization tool described in the previous sections. The calculations were performed assuming natural transition. However, it is not known to what extent the theoretically evaluated laminar flow can be realized for actual airship applications with the occurrence of hull fluttering and surface waviness. Within the transition calculation, a critical amplification factor of $n_{\text{crit}} = 9$ was chosen, which corresponds to a moderate level of turbulence in the freestream.

Five design regimes were chosen, which cover the whole Reynolds number regime relevant for airship applications (Table 1).

The initial source distribution chosen for design regime *I* corresponds to an ellipsoid-like starting geometry with a small

L/D = 2.3 ratio. At first, an optimization run with the commercially available tool POINTER was carried out. Subsequently, a further run with the evolution strategy was performed. For the present investigations with J = 41 design variables, 10.000 generations were chosen for each run, because the adaption time of the covariance matrix is of $\mathbb{O}(J^2)$ generations.[23] Thus, a total of 300,000 designs were generated and analyzed during one optimization run with the (1, 30)-strategy. With consideration of six different Reynolds numbers, the flow evaluation for a single design requires about 2 s CPU time on a SUN ULTRA single-processor workstation.

Figure 6 shows the contour and the inviscid pressure distribution of the best design for regime I. The relatively slender body is characterized by its far aft position of the maximum thickness point and by a moderate, almost constant acceleration upstream of this point. Theoretically, this slightly favorable pressure gradient is sufficient to keep the boundary layer laminar up to 75% of the body length at Reynolds numbers below $Re_V = 3.16 \times 10^6$. The resulting drag curve for the optimized body is shown in Fig. 7. Very low drag coefficients for the whole design regime can be observed. However, if the Reynolds number is only slightly increased above the design region, transition will jump upstream causing an abrupt drag increase. Below $Re_V = 1 \times 10^6$, laminar separation without reattachment is indicated. The drag curve is not plotted for this regime.

An interesting phenomena can be observed for the optimized body. When comparing body contour and pressure distribution, it becomes obvious that the minimum pressure coefficient occurs downstream of the maximum thickness point. Therefore, body contraction started upstream of transition within the design Reynolds number regime. Consequently, the high turbulent skin friction acts on a smaller wetted surface area, thus reducing the viscous drag of the body.

With an increase in Reynolds number the amount of favorable pressure gradient in the forebody region has to be enlarged to maintain laminar flow. This can be realized either by increasing the body diameter or by moving the maximum thickness point upstream. Enlarging the body diameter is limited by the maximum pressure recovery possible without boundary-layer separation in the rear part of the body. The compromise found with the optimization tool for design regime III can be seen in Fig. 8. A steep favorable pressure gradient during the first 50% of the body length is required to achieve extensive laminar flow by shaping alone. The resulting

Table 1 Design regimes

Regime	$Re_{V_{min}}$	$Re_{V_{max}}$	log $Re_{V_{min}}$	log $Re_{V_{max}}$
I	1×10^6	3.16×10^6	6	6.5
II	3.16×10^6	1×10^7	6.5	7
III	1×10^7	3.16×10^7	7	7.5
IV	3.16×10^7	1×10^8	7.5	8
V	1×10^8	3.16×10^8	8	8.5

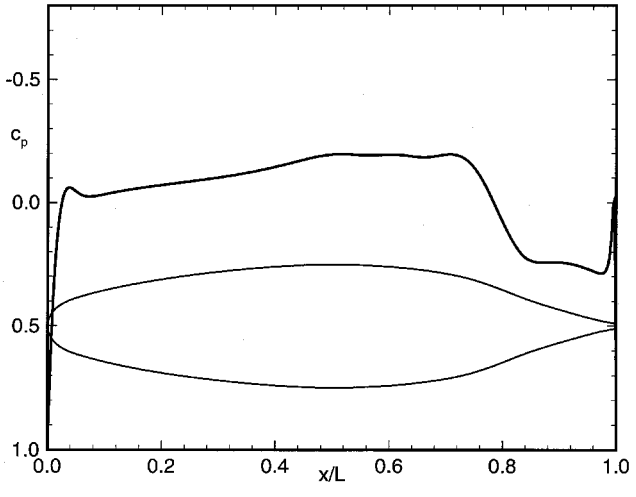

Fig. 6 Inviscid pressure distribution of the body optimized for design regime I.

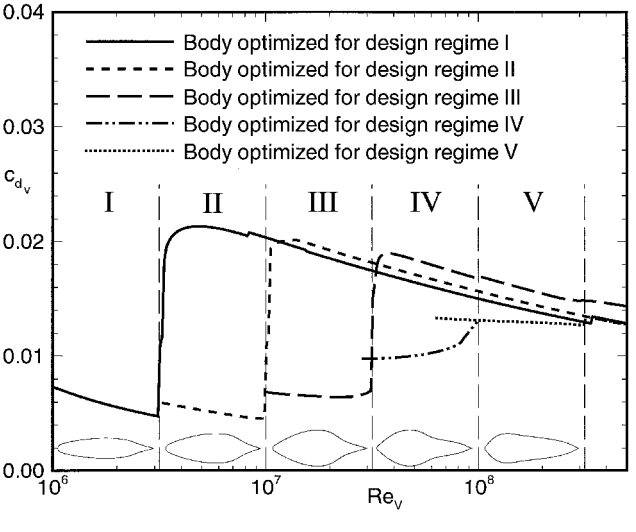

Fig. 7 Drag curve of the optimized body shapes.

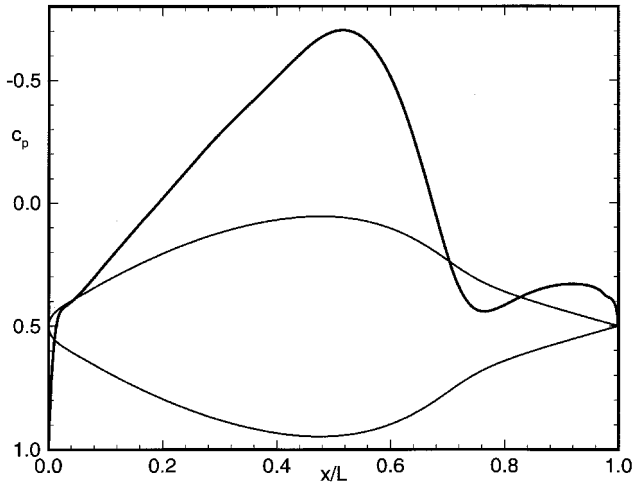

Fig. 8 Inviscid pressure distribution of the body optimized for design regime III.

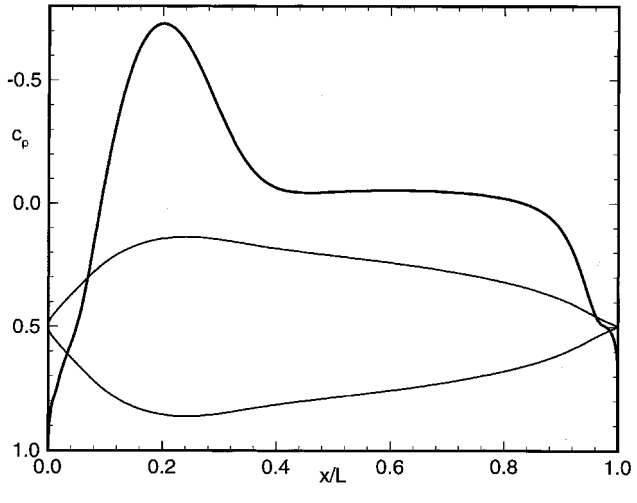

Fig. 9 Inviscid pressure distribution of the body optimized for design regime V.

body again shows a very low drag coefficient for the whole design region (Fig. 7).

Lastly, the contour and the inviscid pressure distribution resulting for the large Reynolds number regime V are shown in Fig. 9. An extremely steep favorable pressure gradient in the forebody region theoretically allows for laminar flow of up to 17% of the body length, even at the upper end of the design regime. The optimized geometry shows an almost pointed nose. However, note that for small angles of attack or sideslip the transition point is expected to move upstream more rapidly than in case of blunt nose shapes.

Drag curves for all optimized bodies are summarized in Fig. 7. It can be seen that the bodies only show favorable behavior inside their respective design regimes. Exact information about the design Reynolds number range is therefore of crucial importance, particularly for the selection of laminar body shapes.

V. Concluding Remarks

A method for numerical shape optimization of axisymmetric bodies at zero incidence submerged in incompressible flow was developed and presented here. Using this method, several bodies, which show minimized drag at maximized volume were designed for different Reynolds number regimes that cover the whole range relevant for airship applications. A semi-empirical e^n method was used for transition prediction within the optimization process for the first time. The results show that up to large Reynolds numbers a certain amount of laminar flow is theoretically possible by adequate shaping of the body contour. To what extent this laminar flow can be realized with the existence of hull fluttering, surface waviness, and roughness of real airships is not yet known. Experiments for solid bodies at lower Reynolds numbers show great sensitivity of the transition location toward surface roughness.

Apart from the shape optimization of the bare hull, additional aspects should be addressed in future investigations. For example, the moment gradient of the envelope plays an important role for the total drag of the configuration, because it determines the size of the fins required to achieve a desired level of static stability. The tool presented will be used for the shape optimization of airship hulls that will take the drag of the required tail surfaces into account. It is also possible to consider other constraints important for a specific airship design, such as hull mass minimization or prescription of a desired center of bouyancy. Finally, implementation of a propeller model should enable aerodynamic optimization of complete airship configurations.

Acknowledgment

The authors thank N. Hansen of Berlin Technical University for providing the optimization algorithm and for his helpful support in conducting the present optimization runs.

References

[1]Gertler, M., "Resistance Experiments on a Systematic Series of Streamlined Bodies of Revolution—for Application to the Design of High Speed Submarines," Navy Dept., Central Air Documents Office, Rept. C-297, Wright–Patterson AFB, Dayton, OH, April 1950.

[2]Carmichael, B. H., "Underwater Drag Reduction Through Optimum Shape," *Proceedings of the AIAA 2nd Propulsion Joint Specialist Conference* (Colorado Springs, CO), AIAA, New York, 1966, pp. 147–169.

[3]Hansen, R. J., and Hoyt, J. G., "Laminar-to-Turbulent Transition on a Body of Revolution with an Extended Favorable Pressure Gradient Forebody," *Journal of Fluids Engineering*, Vol. 106, June 1984, pp. 202–210.

[4]Parsons, J. S., and Goodson, R. E., "Shaping of Axisymmetric Bodies for Minimum Drag in Incompressible Flow," *Journal of Hydronautics*, Vol. 8, No. 3, 1974, pp. 100–107.

[5]Zedan, M. F., Seif, A. A., and Al-Moufadi, S., "Drag Reduction of Airplane Fuselages Through Shaping by the Inverse Method," *Journal of Aircraft*, Vol. 31, No. 2, 1994, pp. 279–287.

[6]Dodbele, S. S., Van Dam, C. P., Vijgen, P. M. H. W., and Holmes, B. J., "Shaping of Airplane Fuselages for Minimum Drag," *Journal of Aircraft*, Vol. 24, No. 5, 1987, pp. 298–304.

[7]Coiro, D. P., and Nicolosi, F., "Design of Natural Laminar Flow Fuselages," *Proceedings of the 19th ICAS Congress* (Anaheim, CA), AIAA, Washington, DC, 1994, pp. 2475–2484.

[8]Pinebrook, W. E., "Drag Minimization on a Body of Revolution," Ph.D. Dissertation, Dept. of Mechanical Engineering, Univ. of Houston, TX, May 1982.

[9]Hess, J. L., and James, R. M., "On the Problem of Shaping an Axisymmetric Body to Obtain Low Drag at Large Reynolds Numbers," Douglas Aircraft Co., Rept. MDC J6791, Long Beach, CA, Jan. 1975.

[10]Lutz, T., Schweyher, H., Wagner, S., and Bannasch, R., "Shape Optimization of Axisymmetric Bodies in Incompressible Flow: Results for the High Reynolds Number Regime," *Proceedings of the 2nd International Airship Conference* (Stuttgart/Friedrichshafen, Germany), ISD, Univ. of Stuttgart, Germany, 1996, pp. 211–224.

[11]Schweyher, H., Lutz, T., and Wagner, S., "An Optimization Tool for Axisymmetric Bodies of Minimum Drag," *Proceedings of the 2nd International Airship Conference* (Stuttgart/Friedrichshafen, Germany), ISD, Univ. of Stuttgart, Germany, 1996, pp. 203–210.

[12]Zedan, M. F., and Dalton, C., "Potential Flow Around Axisymmetric Bodies: Direct and Inverse Problems," *AIAA Journal*, Vol. 16, No. 3, 1978, pp. 242–250.

[13]Eppler, R., and Somers, D. M., "A Computer Program for the Design and Analysis of Low-Speed Airfoils," NASA TM 80210, Aug. 1980.

[14]Young, A. D., "The Calculation of Total and Skin Friction Drags of Bodies of Revolution at Zero Incidence," Aeronautical Research Council, R&M 1874, UK, April 1939.

[15]Mack, L. M., "Boundary Layer Linear Stability Theory," AGARD-AR-709, June 1984.

[16]Würz, W., "Hot-Wire Measurements on Laminar to Turbulent Transition in Attached Boundary Layers and Separation Bubbles and Comparison with Linear Stability Theory and Empirical Transition Criteria," Ph.D. Dissertation, IAG, Univ. of Stuttgart, Germany, 1994.

[17]Smith, A. M. O., and Gamberoni, N., "Transition, Pressure Gradient and Stability Theory," Douglas Rept. ES 26388, El Segundo, CA, 1956.

[18]van Ingen, J. L., "A Suggested Semi-Empirical Method for the Calculation of the Boundary Layer Transition Region," Delft Univ. of Technology, Rept. VTH-74, Delft, The Netherlands, 1956.

[19]Mack, L. M., "A Numerical Method for the Prediction of High-Speed Boundary-Layer Transition Using Linear Theory," NASA SP-347, Jan. 1975.

[20]van Ingen, J. L., and Boermans, L. M. M., "Research on Laminar Separation Bubbles at Delft University of Technology in Relation to Low Reynolds Number Airfoil Aerodynamics," *Proceedings of the Conference on Low Reynolds Number Airfoil Aerodynamics*, Dept. of Aerospace and Mechanical Engineering, Univ. of Notre Dame, Notre Dame, IN, 1985, pp. 89–124.

[21]Schirmer, M., "Aerodynamics Model Tests of German and Foreign Airships in the Zeppelin Wind Tunnel in Friedrichshafen," Ph.D. Dissertation, Technical Univ. Carolo-Wilhelmina, Braunschweig, Germany, 1942.

[22]Rechenberg, I., "Evolution Strategy '94—Workshop Bionics and Evolutiontechnique," Vol. 1, Frommann-Holzboog, Stuttgart, Germany, 1994.

[23]Hansen, N., and Ostermeier, A., "Adapting Arbitrary Normal Mutation Distributions in Evolution Strategies: The Covariance Matrix Adaption," *Proceedings of the 1996 IEEE International Conference on Evolutionary Computation* (Nagoya, Japan), Inst. of Electrical and Electronics Engineers, New York, 1996, pp. 312–317.

[24]Rüger, U., and Kröplin, B., "Aim of Airship Drag Reduction—Optimization Aim and Evaluation Method," *Proceedings of the 2nd International Airship Conference* (Stuttgart/Friedrichshafen, Germany), ISD, Univ. of Stuttgart, Germany, 1996, pp. 191–201.